An Exergy Analysis Model for the Optimal Operation of Integrated Heat-and-Electricity-Based Energy Systems

Jianrun Chen, Haoyong Chen, *Senior Member*, *IEEE*, Zipeng Liang, Xiaodong Zheng, Dongliang Xiao, Yirui Li and Huaguang Yan

***Abstract*—Exergy analysis is a unified approach to evaluating the quantity and quality of energy in integrated energy systems (IESs). However, exergy analysis models have been relatively underexplored for IES operation in energy transmission networks. This study addresses this gap by developing an input-benefit exergy model and an exergy loss calculation model for each link within heat-and-electricity-based IESs (HE-IESs), encompassing the transmission networks. Then, an exergy-based unified optimal operation model for HE-IESs is introduced by minimizing the total exergy loss of the system. In addition, the effect of load rate on the energy efficiency of energy conversion equipment is considered. By applying piecewise linearization to the non-convex terms in the objective function and the equality constraints, the proposed optimization model is accurately and efficiently analyzed as a mixed-integer second-order cone programming problem. The case study results demonstrate that the proposed model reduces equipment-related exergy loss, with approximately 3.2 times the heat network-related exergy loss. Moreover, the average deviation gaps of the overall system's exergy loss and equipment's output exergy power between the proposed and the existing models reach 12.94% and 27.83%, respectively. The maximum relative error of the solution results with the proposed linearization method remains below 1.2%, satisfying the requirements of practical application.**

***Index Terms*—Mixed integer second-order cone programming, integrated energy system, exergy loss, varying energy efficiency, piecewise linearization.**

Received: April 8, 2023
Accepted: October 9, 2023
Published Online: January 1, 2024
Haoyong Chen (corresponding author) is with School of Electric Power Engineering, South China University of Technology, Guangzhou 510640, China (e-mail: eehychen@scut.edu.cn). Zipeng Liang (corresponding author) is with the Department of Electrical Engineering, Hong Kong Polytechnic University, Hong Kong SAR, China (e-mail: liangzipeng.ye@163.com).
DOI: 10.23919/PCMP.2023.000270

I. Introduction

A. Motivations

Current problems associated with energy shortages, climate change, and environmental pollution have generated an urgent need to improve the comprehensive utilization efficiency of energy sources [1], [2]. An important contribution to this effort has focused on coordinating energy production and consumption through the coupling of multiple energy sources, such as electric power, heat, cooling, and renewables, into integrated energy systems (IESs) using energy conversion equipment (ECE) [3]–[5]. For example, the use of ECE components, such as combined heat and power (CHP) systems, has facilitated the development of heat-and-electricity-based IESs (HE-IESs) that meet demands for both heat and electric power with increased overall operational efficiency and flexibility [6], [7].

Among the extensive work conducted for ensuring the optimal operation of IESs, the operating cost of the system has been generally applied as the primary objective of optimization [8]–[12]. However, this limited optimization objective can result in low energy utilization efficiency. This issue is addressed by the energy quality analysis approach conducted via the application of both the first and second laws of thermodynamics. As a result, this analysis approach can reflect the difference in the quality of each energy flow by evaluating the proportion of energy that can be converted into useful work, which is defined as the exergy. Accordingly, an analysis of exergy provides a unified scale for evaluating both the quantity and quality of energy and is therefore more scientific and reasonable than the quantity analysis approach [13].

B. Literature Review

Exergy analysis has been extensively applied in the field of thermodynamic engineering, such as for designing CHP units [14]–[16] and heating, ventilation, and air conditioning (HVAC) systems [17]–[19]. Recent studies have applied exergy analysis in the research on IESs. Faizan et al. have dedicated their efforts to the modeling,

analysis, and evaluation of exergy-based IES. They proposed and developed a smart exergy hub approach to model the electricity, district, and individual heating infrastructure of China for 2020 [20]. Various individual heating scenarios or cases in IESs were compared using exergy and energy analytical methods, facilitating ecologically and economically favorable decisions [21]. Furthermore, a comprehensive review was conducted on applying 4E (energy, exergy, exergoeconomic, and exergoenvironment) analysis in IES, renewable energy, and thermal power plants [22]. Mo et al. analyzed park-level IESs using four exergy-economic indicators: exergy loss, exergy efficiency, exergy loss cost, and exergy-economic coefficient [23]. However, these studies did not address system optimization and analysis of multi-energy networks. Li et al. analyzed the exergy flow distribution mechanism in regional IES networks and proposed a unified exergy flow calculation model for the electricity, heat, and gas networks [24]. This model introduced the concepts of exergy-voltage and exergy-impedance as indicators for evaluating the system's local energy quality. However, this model has not been applied to specific system operation optimization studies. Another study expanded the exergy analysis of heat networks by considering exergy loss within the heat transfer pipes [25]. However, a more complete consideration of the exergy loss in heat networks, including the losses at mixing nodes, is still required for fully optimizing the energy utilization of IESs. Exergy-based optimization studies in IESs have primarily focused on planning research. Hu et al. [26], [27] and Di Somma et al. [28] proposed a single-layer multi-objective planning model for IESs by considering annual exergy efficiency for equipment capacity planning and type selection. In contrast, Wang et al. [29] and Li et al. [30] established a two-layer multi-objective IES planning model, optimizing energy structure and capacity configuration with exergy efficiency at the operational level. However, these studies lack modeling and exergy analysis of the networks. Network layer modeling has previously been considered [26], but the study provides a simplistic representation of network losses by assigning transmission efficiency without incorporating network constraints in the solution methods. In terms of optimizing IES operation through exergy-based methods, Huang et al. [31] and Liu et al. [32] considered system exergy efficiency as an objective and proposed two-stage energy management strategies for HE-IES and day-ahead and real-time operations. However, these studies did not address modeling and analysis of the networks and their losses between energy providers and loads. In addition, the mathematical model and control variables for thermal exergy have not been provided. Chen et al. [33] investigated multi-objective optimization for IES operation based on exergy efficiency, operating cost, and environmental pollution. However, the study considered a simplified thermal exergy expression model without network consideration [33]. Incorporating network modeling adds complexity to exergy analysis but enables a more accurate analysis of the exergy state at different locations within the network.

A significant limitation of existing optimal IES operation models based on exergy is the assumption of constant energy efficiencies for ECE components. Some studies [26], [27], [29] established multi-energy coupling analysis models based on the energy hub [34]. However, the elements representing equipment efficiency in the energy conversion matrix were treated as constants, leading to simplified linear optimization models. Similarly, constant efficiencies of equipment, including CHP, have been assumed in studies [28], [31], [33]. Input-output relationships of other equipment, except for energy storage, were not demonstrated [32]. However, the polynomial relationship between equipment efficiency curves and load rates was considered in one study [30]. Assuming constant efficiencies simplified the model, but it can result in unreasonable IES operation schemes because of varying energy efficiencies of ECE components in accordance with operating conditions, including load rate and environmental parameters, and can only reach maximum values at the rated operating points under standard operational conditions. For example, variations in the load rate can reduce the energy efficiency of the GTs employed in CHP units by up to 37.5% of the maximum efficiency. A more elegant solution was obtained by building an ECE efficiency correction module directly into the IES planning model at the community level to determine the coupling factors as a function of the load rate [35].

Including exergy analysis complicates the optimization model because of the highly nonlinear expression of heat exergy, posing challenges for direction solutions using existing commercial solvers. Therefore, researchers often rely on heuristic algorithms or model simplification. The non-dominated sorting genetic algorithm II (NSGA-II) was previously employed to solve the proposed nonlinear multi-objective optimization problems with exergy efficiency as an objective [27], [29], [31], [32]. Two heuristic algorithms were used in the inner and outer cycles to solve capacity and hourly optimization problems [30]. In addition, a multi-objective particle swarm optimization algorithm was employed [33]. However, heuristic algorithms have drawbacks, such as high computational costs, resources, and time and lack of guaranteed convergence, particularly for greater problem sizes. In addition, the solutions obtained are highly influenced by the algorithm's parameters. Therefore, such algorithms are unsuitable for optimization operations with strict time requirements. Previous studies convexified and solved the network planning problem using the FMINCON solver [26]. Researchers also transformed the optimization model into a linear one by setting the outlet temperature of the collector as a

constant and using the CPLEX solver for the solution [28]. Both approaches simplify the optimization model by fixing the temperature of the heating and cooling loads. In practice, optimization models based on exergy analysis can be approximately treated using methods such as piecewise linearization, which transform the original problem into a suitable type for commercial solvers, enabling efficient and accurate solutions.

C. Study Gaps

The characteristics of existing exergy-based IES studies in the literature review are presented in Table I. Despite the significant contributions of previous research in enhancing the energy efficiency of IESs, some key shortcomings remain as follows:

1) Lack of consideration of network modeling and losses in exergy-based optimization.

2) Insufficient consideration of equipment energy efficiency changes.

3) Inadequately efficient and accurate solution methods for exergy-based operation optimization.

These limitations lead to inaccurate system exergy analysis, unrealistic equipment performance characterization, and low computational efficiency in previous exergy-based IES optimization studies. Consequently, the accuracy of obtained operational strategies, evaluation results, and practicality of the methods is compromised.

D. Contribution

The present work addresses the above-discussed issues by proposing a unified optimal operation model for HE-IESs based on exergy analysis that considers the transmission loss of the exergy flow. The major contributions of this paper are:

1) The model established for analyzing the exergy of HE-IESs includes an input-benefit exergy model and a model for calculating the exergy loss in each link including the networks. It consists of exergy loss models for both the electricity and heat networks and the exergy loss models of ECE, battery storage units, and circulation pumps (CPs). The model enables the minimization of the total exergy loss of the system while also providing the exergy loss distribution of the entire system for detailed analysis and evaluation.

2) The accuracy of the proposed optimization model is enhanced by accounting for the influence of load rates on the efficiencies of ECE components, such as GTs and gas boilers (GBs).

3) The proposed optimization model is analyzed accurately and efficiently as a mixed-integer second-order cone programming (MISOCP) problem by applying piecewise linearization to the non-convex terms in the objective function and the equality constraints.

The remainder of this study is organized as follows. Section II describes the exergy structure of a representative HE-IES and presents the input-benefit exergy model and the model for calculating the exergy loss of an HE-IES. Section III presents the detailed mathematical formulation of the proposed optimization model. Section IV discusses the application of the piecewise linearization method to the optimization model. Section V presents the numerical simulation results, and the paper is concluded in Section VI. The framework of this paper and the interconnections between the sections are illustrated in Fig. 1.

TABLE I
COMPARISON OF EXISTING EXERGY-BASED INTEGRATED ENERGY SYSTEM (IES) RESEARCH WITH THE PROPOSED METHOD

Ref.	Research topics	Network models and losses	Applicability for optimization	Completeness of exergy modeling and analysis	Equipment efficiency	Optimization methods
[20]	Modeling	Not considered	Unavailable	Complete	Constant	
[21] [23]	Analysis / Evaluation	Not considered	Unavailable	Complete	Constant	
[22]	Review of analysis	Not considered	Unavailable	Complete		
[24]	Exergy flow calculation	Thoroughly considered	Unavailable	Complete	Constant	
[25]	Pipeline simulation	Incompletely considered	Unavailable	Complete		
[26]	Planning and efficiency evaluation	Roughly considered	Available	Complete	Constant	Mathematical optimization methods (with simplified model)
[27]	Planning	Not considered	Available	Complete	Constant	Heuristic algorithms
[28]	Planning	Not considered	Available	Complete	Constant	Mathematical optimization methods (with simplified model)
[29]	Planning and efficiency evaluation	Not considered	Available	Complete	Constant	Heuristic algorithms
[30]	Planning and loss evaluation	Not considered	Available	Complete	Variable with load	Heuristic algorithms
[31]–[33]	Operation	Not considered	Available	Incomplete	Constant	Heuristic algorithms
[36]	Operation	Roughly considered	Available	Complete	Constant	Mathematical optimization methods (with approximated model)
This study	**Operation and loss evaluation**	**Thoroughly considered**	**Available**	**Complete**	**Variable with load**	**This study**

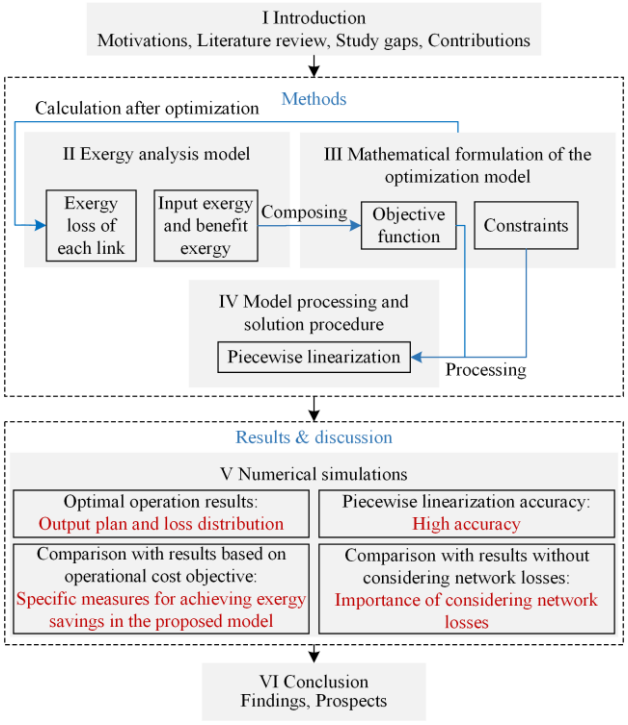

Fig. 1. Framework of this paper.

II. Exergy Analysis Model

The schematic representation and interconnection of the main subsections in this section are illustrated in Fig. 2.

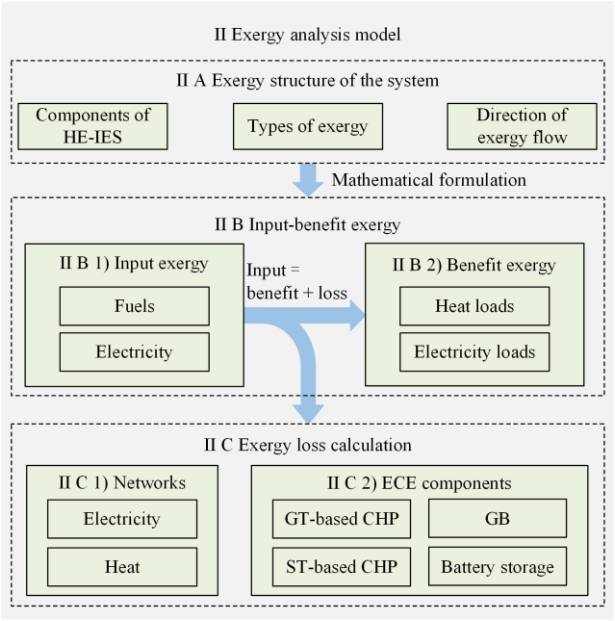

Fig. 2. Composition of the exergy analysis model.

A. Exergy Structure of HE-IESs

An HE-IES mainly consists of electricity and heat loads, electricity and heat networks, network connecting components such as CPs, and ECE components such as CHP units and GBs.

The exergy structure of the representative HE-IES considered in this study is illustrated in Fig. 3. The exergy can be divided into three parts according to the direction of exergy flow: input exergy, exergy loss, and benefit exergy. The portion of the input exergy of the HE-IES that is not lost is converted into benefit exergy for the electric power and heat loads through the ECE components and the electricity and heat networks. The exergy loss represents a reduction in exergy transmission and the exergy of conversion processes.

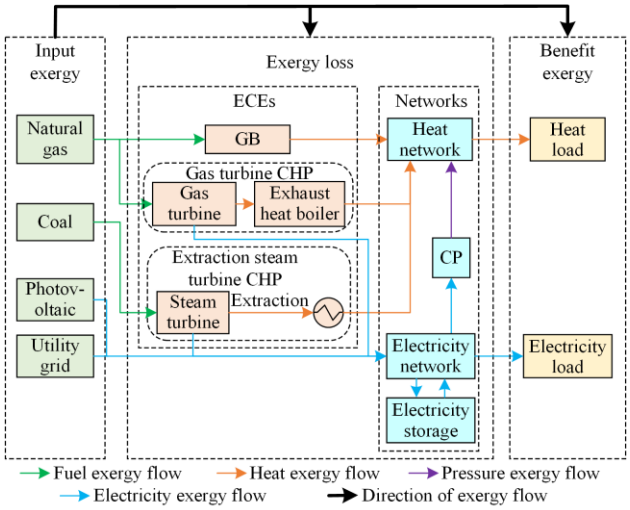

Fig. 3. Exergy structure of a representative integrated heat-and-electricity-based energy system (HE-IES).

B. Models of Input and Benefit Exergy

The input exergy of the HE-IES includes the exergy of natural gas and coal fuels input to the CHP units and GBs, the exergy of photovoltaic (PV) outputs, and the exergy of electricity purchased from an external utility grid. The benefit exergy includes the exergy of electric power and heat outputs to the loads. The difference between the input exergy and the benefit exergy is then defined as the total system exergy loss, which serves as the optimization objective employed in this study.

1) Input Exergy Model

a) Input Exergy of Fuels

The exergy of natural gas and coal fuels $Fx_{ngi,t}$ for a period t can be expressed as:

$$Fx_{ngi,t} = \varepsilon_{fi}\lambda_{fi}F_{ngi,t} \tag{1}$$

where ngi denotes a GT or steam turbine (ST) associated with a CHP unit or a GB; λ_{fi} and ε_{fi} are the calorific value and energy quality coefficient [26], respectively, of a given type of fuel; fi represents natural gas or coal, and $F_{ngi,t}$ is the fuel consumption rate input to unit type ngi during period t.

b) Input Exergy of Electricity

The dead state value of the electricity intensity quantity is 0, which causes the energy quality coefficient of electric power output to be 1. The exergy of electricity is numerically equal to the corresponding

energy of electricity according to energy network theory [37]. Accordingly, the exergy of electricity purchased from an external utility grid $Px_{\mathrm{pur},t}$ and that derived from PV arrays $Px_{\mathrm{pv},t}$ during period t can be expressed as:

$$Px_{\mathrm{pur},t} = P_{\mathrm{pur},t} \tag{2}$$

$$Px_{\mathrm{pv},t} = P_{\mathrm{pv},t} \tag{3}$$

where $P_{\mathrm{pur},t}$ and $P_{\mathrm{pv},t}$ are the electric power purchased from an external utility grid and that output from PV arrays during period t, respectively.

2) Benefit Exergy Model

a) Benefit Exergy of Electricity Loads

According to the above discussion, the exergy of electric power loads ($Px_{\mathrm{load},t}$) during period t is numerically equal to the energy ($P_{\mathrm{load},t}$) of the corresponding electric power loads, which is expressed as:

$$Px_{\mathrm{load},t} = P_{\mathrm{load},t} \tag{4}$$

b) Benefit Exergy of Heat Loads

Heat exergy Qx is defined as the maximum useful work that can be obtained from the heat energy Q provided by a system with a temperature T greater than the ambient temperature T_{a} under given environmental conditions. This is determined by conceiving a series of micro-Carnot heat engines that work between the environment, which serves as a thermal sink, and the system, which serves as a heat reservoir [13]. This can be formalized as:

$$Qx = \int_1^2 (1 - \frac{T_{\mathrm{a}}}{T}) \delta Q = Q - T_{\mathrm{a}} \int_1^2 \frac{\delta Q}{T} \tag{5}$$

where Qx and Q are defined during the process of transitioning from state 1 to state 2. This expression can then be applied to develop expressions for the exergy associated heat loads, the heat outputs of ECE components, and the heat losses of the heat network as follows.

Water at a supply temperature $T_{\mathrm{s,load},t}$ flows into the network node of a heat load during period t and supplies heat to the load through a heat exchanger. The water then flows out of the node and the temperature drops to the so-called outlet temperature $T_{\mathrm{o,load},t}$. Accordingly, the heat exergy of a heat load $\phi x_{\mathrm{load},t}$ during period t can be expressed as:

$$\phi x_{\mathrm{load},t} = C_{\mathrm{p}} m_{\mathrm{q,load},t} \left(T_{\mathrm{s,load},t} - T_{\mathrm{o,load},t} - T_{\mathrm{a}} \ln \frac{T_{\mathrm{s,load},t}}{T_{\mathrm{o,load},t}} \right) \tag{6}$$

where C_{p} is the specific heat capacity of water and $m_{\mathrm{q,load},t}$ is the mass flow rate through the network node of the heat load during period t.

C. Calculation of Exergy Loss

1) Exergy Loss Model of Networks

a) Exergy Loss of an Electricity Network

The exergy loss of electric power lines $\Delta Px_{\mathrm{line},t}$ during period t is numerically equal to the corresponding electric energy loss $\Delta P_{\mathrm{line},t}$ and can therefore be given as:

$$\Delta Px_{\mathrm{line},t} = \Delta P_{\mathrm{line},t} = \sum_{(i,j) \in J} l_{ij,t} R_{ij} \tag{7}$$

where the indices i and j denote an electric power transmission line running from bus i to j in the electricity network; $l_{ij,t}$ is the square of the current running through the (i,j) th transmission line during period t; R_{ij} is the resistance of the (i,j) th transmission line; and J is the set of transmission lines.

The mathematical model defining the active and reactive power outputs of battery storage units can be expressed as [38]:

$$P_{\mathrm{dis},t}^2 + Q_{\mathrm{dis},t}^2 \leqslant S_{\mathrm{pcs,max}}^2 \tag{8a}$$

$$P_{\mathrm{ch},t}^2 + Q_{\mathrm{dis},t}^2 \leqslant S_{\mathrm{pcs,max}}^2 \tag{8b}$$

$$SOC_{\min} \leqslant SOC(t) \leqslant SOC_{\max} \tag{8c}$$

$$SOC(t+1) = (1-\beta) SOC(t) + \eta_{\mathrm{ch}} P_{\mathrm{ch},t} - \frac{P_{\mathrm{dis},t}}{\eta_{\mathrm{dis}}} \tag{8d}$$

$$P_{\mathrm{ch},t} P_{\mathrm{dis},t} = 0 \tag{8e}$$

where $P_{\mathrm{dis},t}$, $P_{\mathrm{ch},t}$, and $Q_{\mathrm{dis},t}$ are the active power values of a battery storage unit associated with discharge and charge and the reactive power associated with discharge at period t, respectively; $S_{\mathrm{pcs,max}}$ is the upper bound of the apparent power of a battery storage unit; $SOC(t)$ is the state of charge of a battery storage unit during period t; $SOC_{\min}$ and $SOC_{\max}$ are the minimal and maximal SOC values for a battery storage unit, respectively; and β, η_{ch}, and η_{dis} are the energy loss coefficient, the charging efficiency, and the discharging efficiency of a battery storage unit, respectively. Equations (8a) and (8b) represent the apparent power limits for battery storage units; (8c) represents the upper and lower limits for the state of charge; (8d) denotes the hourly energy balance equation; and (8e) is used to prevent simultaneous charging and discharging of battery storage.

Therefore, the exergy loss ΔPx_{st} of a battery storage unit during a time horizon T_{t} can be expressed according to the corresponding energy loss ΔP_{st} as:

$$\Delta Px_{\mathrm{st}} = \Delta P_{\mathrm{st}} = \sum_{t=1}^{T_{\mathrm{t}}} \left[\beta SOC(t) + (1-\eta_{\mathrm{ch}}) P_{\mathrm{ch},t} + (1-\eta_{\mathrm{dis}}) \frac{P_{\mathrm{dis},t}}{\eta_{\mathrm{dis}}} \right] \tag{9}$$

b) Exergy Loss of a Heat Network

The heat exergy loss of a heat network mainly occurs via two processes: 1) water in the pipelines of a heat network undergoes convection heat transfer with the environment; 2) water in one pipeline may converge with the water in other pipelines under pressure differences, resulting in heat transfer due to temperature differences at the corresponding network node, which is denoted as a mixing node. Accordingly, the total heat exergy loss of a heat network $\Delta\phi x_t$ during period t can be defined as:

$$\Delta\phi x_t = \Delta\phi x_{\text{pipe},t} + \Delta\phi x_{\text{mix},t} \tag{10}$$

where the heat exergy loss due to convection involving network pipelines $\Delta\phi x_{\text{pipe},t}$ and that due to mixing at mixing nodes $\Delta\phi x_{\text{mix},t}$ during period t can be defined as:

$$\Delta\phi x_{\text{pipe},t} = \sum_{jk\in\Omega_{\text{pipe}}} C_{\text{p}} m_{jk,t}\left(T_{\text{start},jk,t} - T_{\text{end},jk,t} - T_{\text{a}}\ln\frac{T_{\text{start},jk,t}}{T_{\text{end},jk,t}}\right) \tag{11}$$

$$\Delta\phi x_{\text{mix},t} = \sum_{n\in\Omega_{\text{mix}}}\sum_{jn\in\Omega_{in,n}} C_{\text{p}} m_{jn,t} T_{\text{a}}\ln\frac{T_{\text{out},n,t}}{T_{\text{end},jn,t}} \tag{12}$$

where Ω_{pipe} and Ω_{mix} denote the sets of pipelines and mixing nodes of the heat network, respectively; $\Omega_{\text{in},n}$ is the set of pipelines in which the water flows into mixing node n; $m_{jk,t}$ and $m_{jn,t}$ are the mass flow rates within pipeline jk and pipeline jn during period t, respectively; $T_{\text{start},jk,t}$ and $T_{\text{end},jk,t}$ are the temperatures at the first node and the end of pipeline jk during period t; and $T_{\text{out},n,t}$ and $T_{\text{end},jn,t}$ are the temperature of mixing node n and the temperature at the end of pipeline jn during period t, respectively.

The CP induces water flow through the heat network pipelines by converting electric power exergy into pressure exergy. Subsequently, the exergy loss of a CP $Px_{\text{p},t}$ during period t can be expressed as [39]:

$$Px_{\text{p},t} = P_{\text{p},t} = \frac{\sum_{jk\in\Omega_{\text{pipe}}} m_{jk,t} g h_{jk,t}}{10^6\eta_{\text{p}}} \tag{13}$$

where $P_{\text{p},t}$ is the electric power exergy consumed by a CP during period t; $h_{jk,t}$ is the head loss along heat pipeline jk; η_{p} is the energy efficiency of the CP; and g is the acceleration due to gravity. The value of $h_{jk,t}$ can be defined as [39]:

$$h_{jk,t} = \frac{8L_{jk}f_{jk,t}}{D_{jk}^5\rho^2\pi^2 g} m_{jk,t}\left|m_{jk,t}\right| = K_{jk,t} m_{jk,t}\left|m_{jk,t}\right| \tag{14}$$

where ρ is the density of water; L_{jk} is the length and D_{jk} is the diameter of pipeline jk; and $f_{jk,t}$ and $K_{jk,t}$ are the friction factor and resistance coefficient of pipeline jk during period t, respectively.

2) Exergy Loss Model of ECE Components

a) Exergy Loss of GT-based CHPs

A GT-based CHP consists of a GT and an exhaust heat boiler that recovers and heats the waste heat flue gas generated by the GT and supplies the heat to a particular node of the heat network. Therefore, the exergy loss of both the GT and the exhaust heat boiler must be considered in the model.

The energy efficiency of a GT $\eta_{\text{GT,e}}$ exhibits a nonlinear relationship with its load rate. This can be approximated during period t using the following polynomial function [40]:

$$\eta_{\text{GT,e},t} = \sum_{gi=1}^{gn}\alpha_{\text{GT},gi}\left(\frac{P_{\text{GT},t}}{P_{\text{GTN}}}\right)^{gi} \tag{15}$$

where the polynomial whose degree is gn includes a monomial applied within a coefficient $\alpha_{\text{GT},gi}$ of degree gi, which is as an exponent of the ratio of the output power of a GT $P_{\text{GT},t}$ during period t to its rated power P_{GTN}. Therefore, the exergy generated by a GT $Px_{\text{GT},t}$ during period t can be defined as:

$$Px_{\text{GT},t} = P_{\text{GT},t} = \eta_{\text{GT,e},t}\frac{Fx_{\text{GT},t}}{\varepsilon_{\text{gas}}} \tag{16}$$

The heat supplied by the exhaust heat boiler to the given node of the heat network increases the return temperature of the water at that node to the supply temperature. Therefore, the output heat energy $\phi_{\text{GT},t}$ and the output heat exergy $\phi x_{\text{GT},t}$ of an exhaust heat boiler during period t can be obtained as:

$$\phi_{\text{GT},t} = \eta_{\text{GT,h}}\left(\frac{Fx_{\text{GT},t}}{\varepsilon_{\text{gas}}} - P_{\text{GT},t}\right) \tag{17}$$

$$\phi x_{\text{GT},t} = \phi_{\text{GT},t} - C_{\text{p}} m_{\text{q,GT},t} T_{\text{a}}\ln\frac{T_{\text{s,GT},t}}{T_{\text{r,GT},t}} \tag{18}$$

where $\eta_{\text{GT,h}}$ is the collection efficiency; $m_{\text{q,GT},t}$ is the mass flow rate of the node in the heat network that is thermally connected to the GT-based CHP during period t; and $T_{\text{s,GT},t}$ and $T_{\text{r,GT},t}$ are the respective supply and return temperatures at that node during period t.

The exergy loss of a GT-based CHP ($\Delta Ex_{\text{GT},t}$) during period t is the difference between the fuel exergy input to the GT and the sum of the electric power exergy and the heat exergy outputs. This can be expressed as:

$$\Delta Ex_{\text{GT},t} = Fx_{\text{GT},t} - (Px_{\text{GT},t} + \phi x_{\text{GT},t}) \tag{19}$$

b) Exergy Loss of ST-based CHPs

At a given coal consumption rate, the energy efficiency $\eta_{\mathrm{ST,e}}$ of electric power extraction by an ST-based CHP in full condensing mode decreases as the amount of steam extracted increases according to a given ratio Z_{ST} [39]. Accordingly, the electric power exergy $Px_{\mathrm{ST},t}$ and the heat exergy $\phi x_{\mathrm{ST},t}$ output by an ST-based CHP during period t are inter-dependent:

$$Px_{\mathrm{ST},t}=P_{\mathrm{ST},t}=\frac{-\phi_{\mathrm{ST},t}}{Z_{\mathrm{ST}}}+\eta_{\mathrm{ST,e}}\frac{Fx_{\mathrm{ST},t}}{\varepsilon_{\mathrm{coal}}} \tag{20}$$

$$\phi x_{\mathrm{ST},t}=\phi_{\mathrm{ST},t}-C_{\mathrm{p}}m_{\mathrm{q,ST},t}T_{\mathrm{a}}\ln\frac{T_{\mathrm{s,ST},t}}{T_{\mathrm{r,ST},t}} \tag{21}$$

where $P_{\mathrm{ST},t}$ and $\phi_{\mathrm{ST},t}$ are the electric power and heat outputs during period t, respectively; $m_{\mathrm{q,ST},t}$ is the mass flow rate through the node thermally connecting the ST-based CHP with the heat network during period t; and $T_{\mathrm{s,ST},t}$ and $T_{\mathrm{r,ST},t}$ are the respective supply and return temperatures at that node during period t.

As was discussed above for $\Delta Ex_{\mathrm{GT},t}$, the exergy loss of an ST-based CHP $\Delta Ex_{\mathrm{ST},t}$ during period t is:

$$\Delta Ex_{\mathrm{ST},t}=Fx_{\mathrm{ST},t}-(Px_{\mathrm{ST},t}+\phi x_{\mathrm{ST},t}) \tag{22}$$

c) Exergy Loss of GBs

A GB's heat energy extraction efficiency $\eta_{\mathrm{GB},t}$ varies with its load rate and can also be estimated by a polynomial as follows [41]:

$$\eta_{\mathrm{GB},t}=\sum_{bi=1}^{bn}\alpha_{\mathrm{GB},bi}\left(\frac{\phi_{\mathrm{GB},t}}{\phi_{\mathrm{GBN}}}\right)^{bi} \tag{23}$$

$$\phi_{\mathrm{GB},t}=\eta_{\mathrm{GB},t}\frac{Fx_{\mathrm{GB},t}}{\varepsilon_{\mathrm{gas}}} \tag{24}$$

where the polynomial whose degree is bn includes a monomial applied within a coefficient $\alpha_{\mathrm{GB},bi}$ of degree bi, which is as an exponent of the ratio of the output power of a GB $\phi_{\mathrm{GB},t}$ during period t to its rated power ϕ_{GBN}. We note that (23) and (24) are coupled with the terms $\eta_{\mathrm{GB},t}$ and $\phi_{\mathrm{GB},t}$, respectively. Therefore, the exergy generated by a GB $\phi x_{\mathrm{GB},t}$ during period t can be defined as:

$$\phi x_{\mathrm{GB},t}=\phi_{\mathrm{GB},t}-C_{\mathrm{p}}m_{\mathrm{q,GB},t}T_{\mathrm{a}}\ln\frac{T_{\mathrm{s,GB},t}}{T_{\mathrm{r,GB},t}} \tag{25}$$

where $m_{\mathrm{q,GB},t}$ is the mass flow rate through the node thermally connecting the GB with the heat network during period t, and $T_{\mathrm{s,GB},t}$ and $T_{\mathrm{r,GB},t}$ are the respective supply and return temperatures at that node during period t. Subsequently, this equation yields the following expression for the exergy loss of a GB $\Delta Ex_{\mathrm{GB},t}$ during period t:

$$\Delta Ex_{\mathrm{GB},t}=Fx_{\mathrm{GB},t}-\phi x_{\mathrm{GB},t} \tag{26}$$

D. Application Method

The total exergy loss of the system can be quantified into the sum of exergy losses of each link or the disparity between the system's input exergy and the benefit exergy. The former approach offers a more precise assessment of the system losses but necessitates greater computational resources, making it more suitable for post-optimization evaluation. The latter is less precise but only involves solving non-convex input and benefit exergy terms, making it more suitable as the objective function in the optimization model.

III. Mathematical Formulation of the Optimization Model

This section presents the mathematical expressions of each component of the optimization model. An overview of the subsections is shown in Fig. 4.

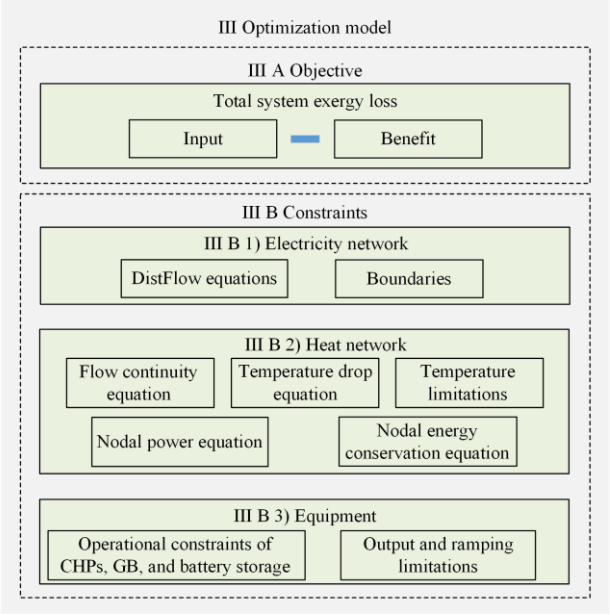

Fig. 4. Composition of the optimization model.

A. Objective Function

The objective function of the unified HE-IES optimization model seeking to minimize the total system exergy loss F can be expressed over a time horizon T_{t} as:

$$\min F=\sum_{t=1}^{T_{\mathrm{t}}}\left(\sum_{ngi}Fx_{ngi,t}+Px_{\mathrm{pur},t}+Px_{\mathrm{pv},t}-Px_{\mathrm{load},t}-\phi x_{\mathrm{load},t}\right) \tag{27}$$

B. Constraints

1) Electricity Network Constraints

The DistFlow equations applied for radial electricity distribution networks are as follows [42]:

$$P_{ij,t}-\sum_{k:(j,k)\in J}P_{jk,t}=P_{j,t}+R_{ij}l_{ij,t} \tag{28}$$

$$Q_{ij,t} - \sum_{k:(j,k)\in J} Q_{jk,t} = Q_{j,t} + X_{ij} l_{ij,t} \tag{29}$$

$$u_{j,t} = u_{i,t} - 2(R_{ij}P_{ij,t} + X_{ij}Q_{ij,t}) + (R_{ij}^2 + X_{ij}^2) l_{ij,t} \tag{30}$$

$$l_{ij,t} u_{i,t} = P_{ij,t}^2 + Q_{ij,t}^2 \tag{31}$$

where $P_{ij,t}$ and $Q_{ij,t}$ respectively denote the real and reactive power transmitted from bus i to bus j during period t; $P_{j,t}$ and $Q_{j,t}$ respectively denote the real and reactive loads at bus j during period t; R_{ij} and X_{ij} are the resistance and reactance of transmission line i,j, respectively; $u_{i,t}$ is the square of the voltage magnitude of bus i; and $l_{ij,t}$ is the square of the current of transmission line i,j during period t.

The quadratic equality in (31) can be derived to the following inequality [43]:

$$l_{ij,t} u_{i,t} \geqslant P_{ij,t}^2 + Q_{ij,t}^2 \tag{32}$$

so that the feasible set of electricity network constraints is convex. In addition, the following limitations must be satisfied:

$$-P_{\mathrm{b,max}} \leqslant P_{ij,t} \leqslant P_{\mathrm{b,max}} \tag{33a}$$

$$-Q_{\mathrm{b,max}} \leqslant Q_{ij,t} \leqslant Q_{\mathrm{b,max}} \tag{33b}$$

$$0 \leqslant l_{ij,t} \leqslant I_{\max}^2 \tag{33c}$$

$$V_{\min}^2 \leqslant u_{i,t} \leqslant V_{\max}^2 \tag{33d}$$

where $P_{\mathrm{b,max}}$, $Q_{\mathrm{b,max}}$, and $I_{\max}$ are the upper bounds of the branch active power, branch reactive power, and branch current, respectively, and $V_{\max}$ and $V_{\min}$ are the respective upper and lower bounds of the voltage magnitude. Equations (33a) and (33b) represent the upper and lower limit constraints for the active and reactive powers of the electricity lines, respectively. Equations (33c) and (33d) denote the upper and lower limits for the square of the current in the electricity lines and the square of the voltage at the nodes, respectively.

2) Heat Network Constraints

The present study applies quality adjustment within the heat network. The constraints of the heat network include hydraulic and heat constraints. The hydraulic constraints include the flow continuity equation. The heat constraints include the nodal power, temperature drop, nodal energy and conservation equations, and temperature limitations [39]. These are presented below.

a) Flow Continuity Equation

$$\boldsymbol{A}\boldsymbol{m}_t = \boldsymbol{m}_{\mathrm{q},t} \tag{34}$$

where $\boldsymbol{A}$ is the network incidence matrix; $\boldsymbol{m}_t$ is a vector defining the mass flow rate within each pipeline during period t; and $\boldsymbol{m}_{\mathrm{q},t}$ is a vector defining the mass flow rate through each node injected from a supply or discharged to a load during period t.

b) Nodal Power Equation

$$\phi_{n,t} = C_{\mathrm{p}} m_{\mathrm{q},n,t} (T_{\mathrm{s},n,t} - T_{\mathrm{o},n,t}) \tag{35}$$

where $\phi_{n,t}$ is the heat consumed or supplied at node n during period t, $m_{\mathrm{q},n,t}$ is the mass flow rate through node n during period t, and $T_{\mathrm{s},n,t}$ and $T_{\mathrm{o},n,t}$ are the respective supply and outlet temperatures at node n during period t.

c) Temperature Drop Equation

$$(T_{\mathrm{end},jk,t} - T_{\mathrm{a}}) = (T_{\mathrm{start},jk,t} - T_{\mathrm{a}}) e^{-\frac{\lambda_{\mathrm{h},jk} L_{jk}}{C_{\mathrm{p}} m_{jk,t}}} \tag{36}$$

where $\lambda_{\mathrm{h},jk}$ is the overall heat transfer coefficient of pipeline jk per unit length.

d) Nodal Energy Conservation Equation

$$(\sum m_{\mathrm{out},n,t}) T_{\mathrm{out},n,t} = \sum m_{\mathrm{in},n,t} T_{\mathrm{in},n,t} \tag{37}$$

where $m_{\mathrm{out},n,t}$ is the mass flow rate within a pipeline leaving node n, $m_{\mathrm{in},n,t}$ is the mass flow rate within a pipeline coming into node n during period t, and $T_{\mathrm{in},n,t}$ is the water temperature at the end of a pipeline at node n and period t.

e) Temperature Limitations

$$T_{\mathrm{s,min}} \leqslant T_{\mathrm{s},n,t} \leqslant T_{\mathrm{s,max}} \tag{38a}$$

$$T_{\mathrm{o,min}} \leqslant T_{\mathrm{o},n,t} \leqslant T_{\mathrm{o,max}} \tag{38b}$$

$$T_{\mathrm{r,min}} \leqslant T_{\mathrm{r},n,t} \leqslant T_{\mathrm{r,max}} \tag{38c}$$

where $T_{\mathrm{s,max}}$ and $T_{\mathrm{s,min}}$ are the respective upper and lower bounds of the supply temperature, $T_{\mathrm{o,max}}$ and $T_{\mathrm{o,min}}$ are the respective upper and lower bounds of the outlet temperature, and $T_{\mathrm{r,max}}$ and $T_{\mathrm{r,min}}$ are the respective upper and lower bounds of the return temperature. Equations (38a), (38b), and (38c) represent the upper and lower limits for the node supply, outlet, and return temperatures, respectively.

3) Equipment Constraints

The operational constraints of a GT-based CHP, ST-based CHP, GB, and a battery storage unit are respectively given as (15)–(17), (20) and (21), (23) and (24), and (8a)–(8e). The limitations applied to the equipment output power and up/down ramping power at each time interval are considered to be:

$$P_{\mathrm{GT,min}} \leqslant P_{\mathrm{GT},t} \leqslant P_{\mathrm{GT,max}} \tag{39a}$$

$$P_{\mathrm{ST,min}} \leqslant P_{\mathrm{ST},t} \leqslant P_{\mathrm{ST,max}} \tag{39b}$$

$$\phi_{\mathrm{GB,min}} \leqslant \phi_{\mathrm{GB},t} \leqslant \phi_{\mathrm{GB,max}} \tag{39c}$$

$$-P_{\mathrm{GT,down}} \leqslant P_{\mathrm{GT},t+1} - P_{\mathrm{GT},t} \leqslant P_{\mathrm{GT,up}} \tag{39d}$$

$$-P_{\mathrm{ST,down}} \leqslant P_{\mathrm{ST},t+1} - P_{\mathrm{ST},t} \leqslant P_{\mathrm{ST,up}} \tag{39e}$$

$$-\phi_{\mathrm{GB,down}} \leqslant \phi_{\mathrm{GB},t+1} - \phi_{\mathrm{GB},t} \leqslant \phi_{\mathrm{GB,up}} \tag{39f}$$

$$0 \leqslant P_{\mathrm{ch},t} \leqslant P_{\mathrm{ch,max}} \tag{39g}$$

$$0 \leqslant P_{\mathrm{dis},t} \leqslant P_{\mathrm{dis,max}} \tag{39h}$$

where $P_{\mathrm{GT,max}}$ and $P_{\mathrm{GT,min}}$ are the respective upper and lower bounds of the electric power output of GTs; $P_{\mathrm{GT,up}}$ and $P_{\mathrm{GT,down}}$ are the respective maximum up-ramping power and down-ramping power of GTs; $P_{\mathrm{ST,max}}$ and $P_{\mathrm{ST,min}}$ are the respective upper and lower bounds of the electric power output of STs; $P_{\mathrm{ST,up}}$ and $P_{\mathrm{ST,down}}$ are the respective maximum up-ramping power and down-ramping power of STs; $\phi_{\mathrm{GB,max}}$ and $\phi_{\mathrm{GB,min}}$ are the respective upper and lower bounds of the heat output of GBs; $\phi_{\mathrm{GB,up}}$ and $\phi_{\mathrm{GB,down}}$ are the respective maximum up-ramping power and down-ramping power of GBs; and $P_{\mathrm{ch,max}}$ and $P_{\mathrm{dis,max}}$ are the upper bounds for the rates of battery storage unit charging and discharging, respectively. Equations (39a), (39b), and (39c) denote the upper and lower limits for the output of GT, ST, and GB, respectively. Equations (39d), (39e), and (39f) represent the ramping constraints for GT, ST, and GB, respectively. Equations (39g) and (39h) represent the upper and lower limits for the charging and discharging of battery storage, respectively.

IV. Model Processing and Solution Procedure

The logarithmic term in (6) makes the objective function non-convex, and model components (16), (24), and (8e) are all nonlinear. Therefore, the optimization model is non-convex and difficult to solve. This issue is addressed by applying piecewise linearization to the objective function and the nonlinear equality constraints and introducing binary variables, transforming the original problem into an MISOCP problem. The resulting problem can be solved using the Gurobi Solver in the MATLAB platform and the YALMIP toolbox. The schematic diagram of the piecewise linearization method is shown in Fig. 5.

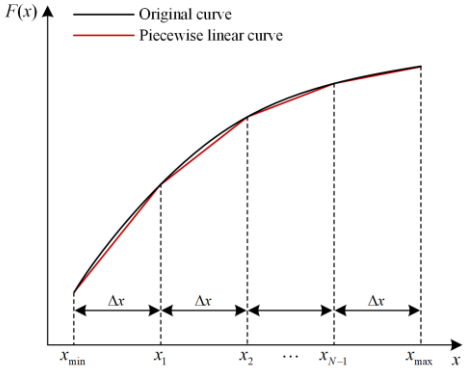

Fig. 5. Piecewise linearization of the non-convex terms.

A. Piecewise Linearization of the Heat Load Exergy

Applying piecewise linearization to the functions $\ln T_{\mathrm{s,load},t}$ and $\ln T_{\mathrm{o,load},t}$ in (6) enables $\phi x_{\mathrm{load,t}}$ to be defined by the following linear form:

$$\phi x_{\mathrm{load,t}} = C_{\mathrm{p}} m_{\mathrm{q,load},t}(T_{\mathrm{s,load},t} - T_{\mathrm{o,load},t}) - C_{\mathrm{p}} m_{\mathrm{q,load},t} T_{\mathrm{a}} \left(\sum_{li}^{N_{\mathrm{fs}}} \gamma_{\mathrm{s},li} T_{\mathrm{s,load},t,li} - \sum_{lj}^{N_{\mathrm{fo}}} \gamma_{\mathrm{o},lj} T_{\mathrm{o,load},t,lj} + \ln \frac{T_{\mathrm{s,min}}}{T_{\mathrm{o,min}}} \right) \tag{40}$$

where N_{fs} and N_{fo} are the numbers of segments into which the functions $\ln T_{\mathrm{s,load},t}$ and $\ln T_{\mathrm{o,load},t}$ have been respectively divided within the upper and lower bounds of their ranges; $\gamma_{\mathrm{s},li}$ and $\gamma_{\mathrm{o},lj}$ are the slopes of the *li*th segment of $\ln T_{\mathrm{s,load},t}$ and the *lj*th segment of $\ln T_{\mathrm{o,load},t}$, respectively; and $T_{\mathrm{s,load},t,li}$ and $T_{\mathrm{o,load},t,lj}$ are the values of the *li*th segment of $T_{\mathrm{s,load},t}$ and the *lj*th segment of $T_{\mathrm{o,load},t}$, respectively. In addition, the variables introduced by piecewise linearization are subject to the following constraints:

$$T_{\mathrm{s,min}} + \sum_{li}^{N_{\mathrm{fs}}} T_{\mathrm{s,load},t,li} = T_{\mathrm{s,load},t} \tag{41a}$$

$$T_{\mathrm{o,min}} + \sum_{lj}^{N_{\mathrm{fo}}} T_{\mathrm{o,load},t,lj} = T_{\mathrm{o,load},t} \tag{41b}$$

$$I_{\mathrm{s},t,li+1}\Delta s \leqslant T_{\mathrm{s,load},t,li} \leqslant I_{\mathrm{s},t,li}\Delta s \tag{41c}$$

$$I_{\mathrm{o},t,lj+1}\Delta o \leqslant T_{\mathrm{o,load},t,lj} \leqslant I_{\mathrm{o},t,lj}\Delta o \tag{41d}$$

where $I_{\mathrm{s},t,li}$ and $I_{\mathrm{o},t,lj}$ are binary variables, and Δs and Δo are the segment lengths of $T_{\mathrm{s,load},t}$ and $T_{\mathrm{o,load},t}$, respectively. Equations (41a) and (41b) represent the relationships between the supply and outlet temperatures of the load side and their corresponding piecewise variables, respectively. Equations (41c) and (41d) represent the constraining relationships between each segment's piecewise variables.

B. Piecewise Linearization of the ECE Models

As was applied for the heat load exergy, the GT and GB models in (16) and (24) can be replaced by the following linear models, and the explanation of each constraint is omitted here.

$$\begin{cases} Fx_{\mathrm{GT},t} = \varepsilon_{\mathrm{gas}} \left(\sum_{ei}^{N_{\mathrm{GT}}} \gamma_{\mathrm{GT},t,ei} P_{\mathrm{GT},t,ei} + \dfrac{P_{\mathrm{GT,min}}}{\eta_{\mathrm{GT,e,min}}} \right) \\ P_{\mathrm{GT,min}} + \sum_{ei}^{N_{\mathrm{GT}}} P_{\mathrm{GT},t,ei} = P_{\mathrm{GT},t} \\ I_{\mathrm{GT},t,ei+1}\Delta T \leqslant P_{\mathrm{GT},t,ei} \leqslant I_{\mathrm{GT},t,ei}\Delta T \\ Fx_{\mathrm{GB},t} = \varepsilon_{\mathrm{gas}} \left(\sum_{hi}^{N_{\mathrm{GB}}} \gamma_{\mathrm{GB},t,hi} \phi_{\mathrm{GB},t,hi} + \dfrac{\phi_{\mathrm{GB,min}}}{\eta_{\mathrm{GB,min}}} \right) \\ \phi_{\mathrm{GB,min}} + \sum_{hi}^{N_{\mathrm{GB}}} \phi_{\mathrm{GB},t,hi} = \phi_{\mathrm{GB},t} \\ I_{\mathrm{GB},t,hi+1}\Delta B \leqslant \phi_{\mathrm{GB},t,hi} \leqslant I_{\mathrm{GB},t,hi}\Delta B \end{cases} \tag{42}$$

where N_{GT} and N_{GB} are the numbers of segments into which the functions $P_{GT,t}/\eta_{GT,e,t}$ and $\phi_{GB,t}/\eta_{GB,t}$ have been respectively divided within the upper and lower bounds of their ranges; $\gamma_{GT,t,ei}$ and $\gamma_{GB,t,hi}$ are the slopes of the *ei*th segment of $P_{GT,t}/\eta_{GT,e,t}$ and the *hi*th segment of $\phi_{GB,t}/\eta_{GB,t}$, respectively; $P_{GT,t,ei}$ and $\phi_{GB,t,hi}$ are the values of the *ei*th segment of $P_{GT,t}$ and the *hi*th segment of $\phi_{GB,t}$, respectively; $\eta_{GT,e,min}$ and $\eta_{GB,min}$ are the minimum efficiencies of GTs and GBs, respectively; $I_{GT,t,ei}$ and $I_{GB,t,hi}$ are binary variables; and ΔT and ΔB are the segment lengths of $P_{GT,t}$ and $\phi_{GB,t}$, respectively.

Finally, (8e) is treated as the following constraints using binary variables $I_{ch,t}$ and $I_{dis,t}$:

$$\begin{cases} 0 \leqslant P_{ch,t} \leqslant I_{ch,t} P_{ch,max} \\ 0 \leqslant P_{dis,t} \leqslant I_{dis,t} P_{dis,max} \\ I_{ch,t} + I_{dis,t} \leqslant 1 \end{cases} \tag{43}$$

V. Numerical Simulations

This section presents numerical simulations to validate the effectiveness of the proposed model and method. A comprehensive description of the composition, structure, parameters, and information of the test system is provided. Subsequently, the simulation results are presented and analyzed, encompassing the optimal system operation based on minimum exergy loss and loss distribution, the precision of the piecewise linearization method, and a comparative analysis of the conventional operational cost-based optimizing approach and the exergy-based optimal operation approach that disregards network losses.

A. Description of the Simulation System

The test HE-IES used in the simulations included a 32-node district heating network and a modified IEEE 33-bus electric power system. Both systems are illustrated in Fig. A1 of Appendix A. The parameters of the ECE components and other equipment parameters of the HE-IES are listed in Table A1 of Appendix A, and the parameters applied for the pipelines in the heat network are listed in Table A2 of Appendix A. The time horizon employed in all simulations was $T_t = 24$ h and the difference between time periods Δt was 1 h.

In the electricity network, bus 33 was set as the slack bus, the baseline voltage was set as $V_b = 11$ kV, and the voltage range of the remaining buses was set as [0.93, 1.07] p.u. The typical curves applied for the electric loads and PV power outputs are shown in Fig. 6. The maximum allowable power purchased from the external utility grid was set as $P_{pur,max} = 3.5$ MW.

In the heat network, node 1 was set as the slack node, the supply temperature range was set as [60, 100]°C, the outlet and return temperature ranges were both [30, 55]°C, and the other pertinent constants were set as follows: $\rho = 959.488$ kg/m^3, $g = 9.8$ m/s^2, $C_P = 4.182$ kJ/(kg K), $\lambda_{gas} = 10.45$ (kWh)/m^3, the value of ε_{gas} was set within the range 0.6219–0.6270 according to the assigned ambient temperature, $\lambda_{coal} = 8.14$ kWh/kg, and the value of ε_{coal} was set within the range 0.4381–0.4451 according to the assigned ambient temperature. The piecewise linearization parameters were $N_{fs} = N_{fo} = 4$ and $N_{GT} = N_{GB} = 4$.

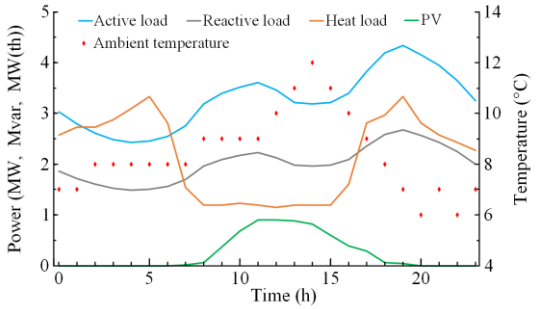

Fig. 6. Typical load, PV output, and ambient temperature curves applied in the simulations.

B. Simulation Results

1) Optimal HE-IES Operation

The electric power and heat exergy outputs obtained for the main equipment in the HE-IES optimized according to the total exergy loss of the system are presented in Figs. 7 and 8, respectively. We note from Fig. 7 that the electric power exergy outputs of the two CHP units exhibit opposite trends. This is because the two CHP units require opposite output characteristics to meet the heat load. The electric power and heat outputs of the GT-based CHP2 increase with increasing fuel input rate, whereas the electric power and heat outputs of the ST-based CHP1 exhibit a negative linear correlation. Most of the electric load and its variations are met by purchasing electricity from the utility grid. As can be seen from Fig. 8, the heat exergy efficiencies of ECE components are all less than 23%, indicating that the energy level of the heat is low [26].

An analysis of the trends observed in Figs. 7 and 8 over time indicates that the electric exergy efficiency of CHP2 varied greatly according to variations in the electric power load. During the intervals 00:00–04:00 and 18:00–23:00, the electric exergy efficiency of CHP2 was at a high level and the fuel input rate of CHP2 was also high. Accordingly, the heat exergy output of CHP2 was greater than that of CHP1 during these intervals. During the interval 07:00–16:00, CHP2 exhibited a reduced electric exergy efficiency and the heat output was re-

duced. However, CHP2 gradually reduced its heat exergy output during 03:00–06:00 to meet the low heat load in the subsequent period because of the ramping power constraints of the unit. Then, CHP2 gradually increased its heat output between 16:00 and 17:00 to meet the high heat load in the subsequent period. For the other system components, the results in Fig. 8 for the GB as a whole indicate that, although the GB provides a high heat production efficiency, its total exergy efficiency is much less than the efficiencies of the two CHPs. Therefore, its heat exergy output is less than that of the two CHPs. The results in Fig. 7 indicate that the battery storage units tend to reduce the exergy loss of the electricity network by being charged during periods of low electric load and discharged during peak electric load periods. In addition, the battery storage units are charged at the end of the time horizon to ensure that they can continuously participate in regulating the electricity network within the next time horizon. However, the complementary output trends of the two CHPs have the most profound effect on the overall operational efficiency of the HE-IES during the time horizon. These trends keep the total exergy loss of all equipment at a low level while maintaining the balance of supply and demand.

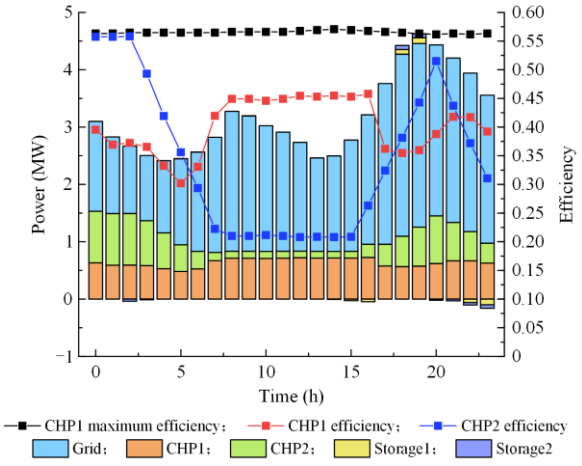

Fig. 7. Electric exergy outputs and efficiencies of equipment in the HE-IES.

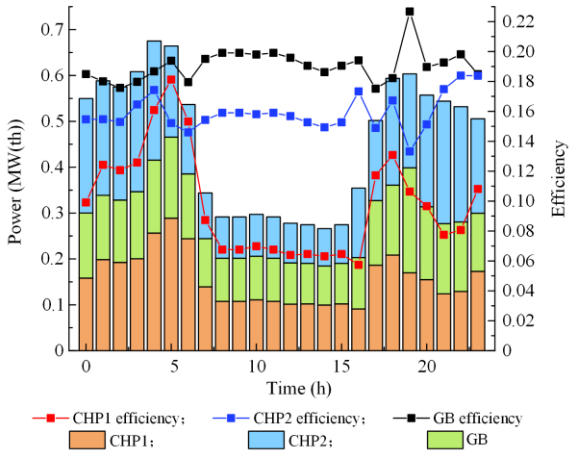

Fig. 8. Heat exergy outputs and efficiencies of equipment in the HE-IES.

Details regarding the calculated distributions of exergy and energy losses at each link in the HE-IES are presented in Table II. These results enable a detailed analysis of both the exergy loss distribution of the system and a comparison of the exergy and energy losses of each component in the system.

The results in the table indicate that the exergy loss of the ECE components accounts for most of the total exergy loss of the system. Accordingly, we can conclude that more exergy is lost in the energy conversion process than in the energy transmission process. In particular, the exergy loss of CHP1 accounts for a very large percentage of the total exergy loss of all ECE components because of the low power generation efficiency of the ST. With respect to the energy transmission process, the exergy loss of the electricity network is greatest owing to the high-quality characteristic of electrical energy. Meanwhile, the heat supply network exhibits a greater exergy loss than the return network because of the greater supply temperature and wider range of variation than the return temperature. Consequently, there is a higher exergy loss caused by convection heat transfer in pipelines and heat transfer resulting from temperature differences at mixing nodes of the supply network.

Comparing the exergy loss and energy loss of the system, we find that the exergy loss of CHP2 is greater than its energy loss, while the exergy loss of CHP1 is less than its energy loss. This is because the proportion of fuel exergy contained in coal is less than that of natural gas, and the input exergy is also less for the same input energy. We further note that the energy loss of the GB is small, and its proportion is small owing to its high energy efficiency. However, its exergy loss represents a much larger proportion of the total exergy loss because the energy level of heat is low. Similarly, the low-quality characteristic of heat energy causes the heat network's exergy loss, accounting for a relatively small proportion of the total exergy loss. Moreover, its exergy loss is found to be less significant compared to its energy loss. The energy loss of the heat network is even greater than that of certain ECE components, such as GB and CHP2. These factors indicate that although the energy loss in the energy transmission process occupies a relatively large proportion of the total, most of the energy loss is due to energy that cannot be converted into useful work. Therefore, the exergy loss in the energy transmission process accounts for a relatively small proportion of the total exergy loss of the system.

TABLE II
DISTRIBUTIONS OF EXERGY AND ENERGY LOSSES IN THE HE-IES

Loss links	Exergy loss (MWh)	Exergy loss proportion (%)	Energy loss (MWh)	Energy loss proportion (%)
GB	13.1696	26.14	3.2172	4.04
CHP2	11.7012	23.23	6.2844	7.89
CHP1	19.1068	37.93	47.3079	59.39
Supply network	2.3713	4.71	12.5368	15.74
Return network	0.8649	1.72	7.1481	8.97
Electricity network	2.9432	5.84	2.9432	3.69
Battery storage	0.1208	0.24	0.1208	0.15
CP	0.0964	0.19	0.0964	0.12
Total	50.3743	100	79.6549	100

2) Analysis of Piecewise Linearization Accuracy

The relative errors caused by applying piecewise linearization to the heat load exergy and the equipment models over the 24 h time horizon are presented in Fig. 9. We note that the relative errors are quite small, and a maximum relative error of only about 1.2% is observed. Accordingly, we can conclude that the piecewise linearization method employed in this paper provided high calculation accuracy.

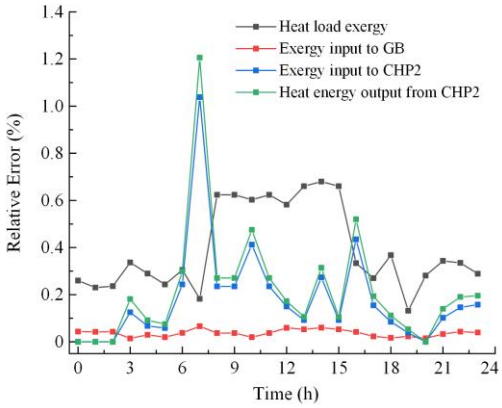

Fig. 9. Relative errors caused by piecewise linearization.

3) Comparison of Optimal Results Obtained with Two Different Objective Functions

The optimal results obtained using the proposed objective function that seeks to minimize the total exergy loss of the HE-IES were compared with those obtained using an objective function that seeks to minimize the operational cost of the system. The objective function applied for minimizing the total operational cost G of the HE-IES during the 24 h time horizon is given by:

$$\begin{cases} \min G = \sum_{t=1}^{T_t} (C_{\mathrm{GB},t} + C_{\mathrm{GT},t} + C_{\mathrm{ST},t} + C_{\mathrm{pur},t}) \\ C_{\mathrm{GB},t} = c_{\mathrm{g}} F_{\mathrm{GB},t} \\ C_{\mathrm{GT},t} = c_{\mathrm{g}} F_{\mathrm{GT},t} \\ C_{\mathrm{ST},t} = c_{\mathrm{c}} F_{\mathrm{ST},t} \\ C_{\mathrm{pur},t} = c_{\mathrm{pur}} P_{\mathrm{pur},t} \end{cases} \tag{44}$$

where $C_{\mathrm{GB},t}$, $C_{\mathrm{GT},t}$, $C_{\mathrm{ST},t}$, and $C_{\mathrm{pur},t}$ are the costs associated with the GB, GT-based CHP, ST-based CHP, and purchasing electricity from the utility grid, respectively, where c_{g} is the unit price of natural gas ($c_{\mathrm{g}} = 2.5$ ¥/m^3), c_{c} is the unit price of standard coal ($c_{\mathrm{c}} = 1200$ ¥/t), and c_{pur} is the electricity purchase price, which is defined herein as a function of time according to the curve shown in Fig. 10. The constraints applied for this optimization model are equivalent to those applied for the proposed optimization model discussed in Subsection III B.

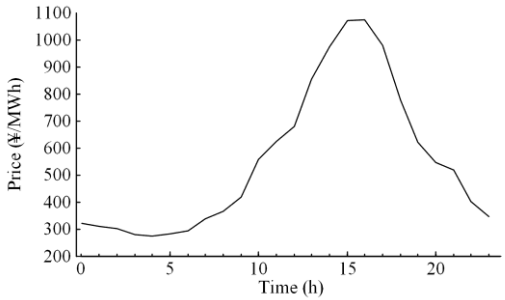

Fig. 10. Electricity purchase price curve.

The electric power and heat exergy outputs obtained for the main equipment in the HE-IES optimized according to the two objectives are presented in Figs. 11 and 12, respectively. The differences between the two objectives are clearly conveyed by comparing the electricity purchased from the external grid and the outputs of CHP2 during the period of low electricity price in the interval of 00:00–06:00. Here, the operational cost perspective favors a low electricity price by increasing the electricity purchased from the utility while simultaneously decreasing the electricity output of CHP2 because the production cost of CHP2 is greater than the cost of purchasing electricity from the utility. Meanwhile, the operational cost perspective employs CHP1 to maintain a balance between heat supply and demand by reducing its electricity output while increasing its heat output. Conversely, the operational cost perspective reduces the electricity purchased from the utility during periods of high electricity price, such as between 13:00 and 17:00, increases the electricity output of CHP2, and employs CHP1 to maintain the balance between heat supply and demand by reducing its heat output while increasing its electricity output. The operational cost perspective also increases the frequency of charging and discharging for the battery storage units. The economy is served by charging during periods of low electricity prices and discharging during periods of high electricity prices.

In general, the optimization results with the minimum exergy loss objective have a greater exergy output. This increase causes the ECE to have higher exergy efficiencies, thereby reducing the exergy loss of the ECE.

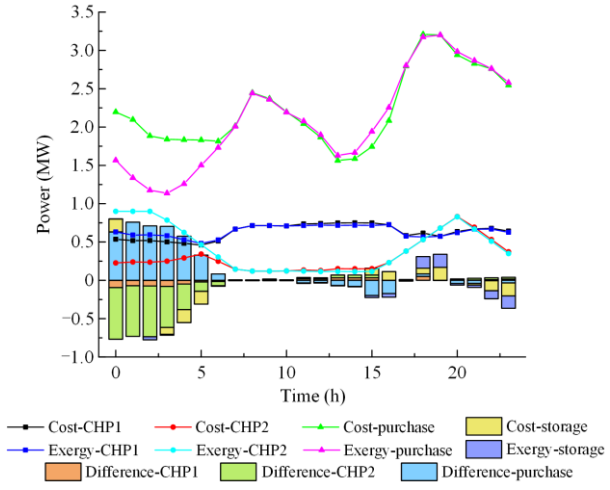

Fig. 11. Comparison of electric power exergy outputs obtained with the two objectives.

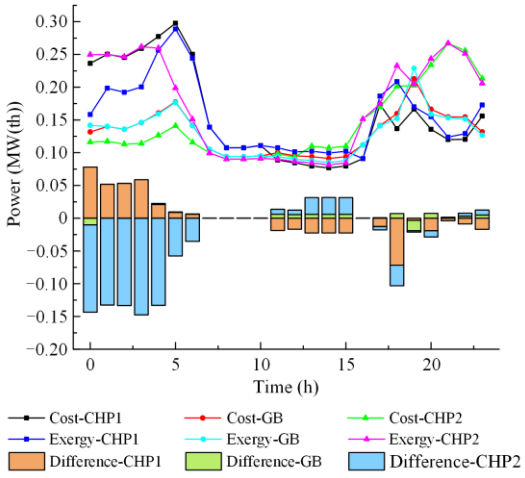

Fig. 12. Comparison of heat exergy outputs obtained with the two objectives.

Details regarding the calculated distribution of exergy loss obtained at each link in the HE-IES with the two objectives are presented in Table III. These results demonstrate that the exergy losses of battery storage units, GB, CHP1, CHP2, and the electricity network obtained under the minimum operational cost objective are greater than those obtained under the minimum exergy loss objective, while the exergy losses of the supply and return networks are slightly less. While one would expect decreased exergy losses under the minimum exergy loss objective, the increased exergy loss of the heat network is somewhat surprising. This change can be attributed to the constant difference between the supply and return temperatures at the node where an ECE is situated for a given heat energy output, as indicated by (35). Furthermore, an increase in the supply and return temperatures leads to an increase in the heat exergy output of the ECE, as illustrated by (18), (21), and (25). Consequently, this increase causes a reduction in the exergy loss of the ECE. However, this condition increases the temperature drop in the heat network according to (36), which leads to greater exergy loss in the heat network. This analysis is verified by the results in Fig. 13 for CHP2 as an example, where the supply and return temperatures of CHP2 obtained with the two objectives are plotted over the 24 h time horizon. It can be seen that the maximum values of the supply and return temperatures obtained under the minimum exergy loss objective are greater than those obtained under the minimum operational cost objective. Therefore, the optimization obtained with the minimum total system exergy loss objective is essentially a trade-off between reducing the exergy loss of the equipment and increasing the exergy loss of the heat network, thereby minimizing the total exergy loss while meeting the energy requirements of the loads. The simulation results show that the reduced exergy loss of the equipment is 0.6692 MWh, about 3.2 times the increased exergy loss of the heat network (0.2096 MWh).

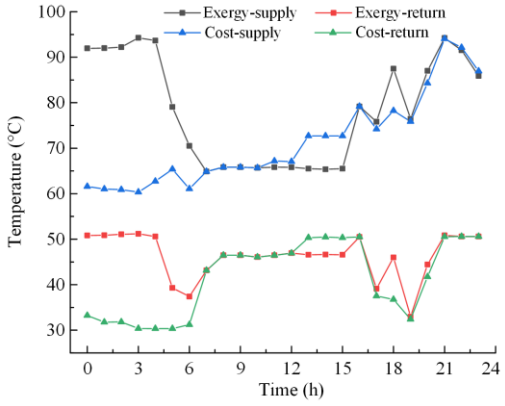

Fig. 13. Comparison of the supply and return temperatures of the GT-based CHP with the two objectives.

TABLE III
COMPARISON OF THE EXERGY LOSS RESULTS OBTAINED AT EACH LINK WITH THE TWO OBJECTIVES

Objective	Exergy loss (MWh)								
	Battery storage units	GB	CHP2	CHP1	Supply network	Return network	Electricity network	CP	Total
Operational cost	0.1763	13.2559	12.1063	19.2291	2.2421	0.7845	3.0340	0.0964	50.9246
Exergy loss	0.1208	13.1696	11.7012	19.1068	2.3713	0.8649	2.9432	0.0964	50.3742

A comparison of the operational costs obtained for the HE-IES with the two objectives is presented in Table IV. We note that the costs associated with system operation obtained under the minimum operational cost objective

are nearly all greater or the same as those obtained under the minimum total system exergy loss objective, particularly the cost of electricity purchased from the external grid. However, the smaller total operational cost of the system obtained from the operational cost perspective is the result of the greatly reduced cost of 1202.68 ¥ associated with CHP2 operation. With the objective of minimizing exergy cost, the utilization rate of equipment in CHP2 increased by approximately 13.76% compared to the objective of minimizing operational loss. This observation highlights the significance of optimizing for exergy loss, as it facilitates comprehensive utilization of ECE. These results, in conjunction with the results presented previously, demonstrate that the reduced total operational cost obtained with the minimum operational cost objective is generally achieved by increasing the volume of electricity purchased from the external grid during low electricity price periods and reducing the utilization of the GT-based CHP.

This paper proposes an optimization model from the perspective of efficient resource utilization (exergy utilization) that has been rarely addressed in previous studies and that may lead to a slight increase in system cost while improving energy utilization. Compared with the multi-objective optimization method that comprises cost and exergy loss and seeks a compromise solution, exergic economics can adequately illustrate the relationship between energy quality (exergy) and operational cost, thereby offering a more theoretical basis for the prices of various exergy flows, so that a more accurate economy of energy use can be achieved. Therefore, the use of exergy economics in optimizing IESs requires further investigation.

TABLE IV
COMPARISON OF OPERATIONAL COSTS OBTAINED UNDER THE TWO OBJECTIVES

Objective	Cost (¥)				
	Electricity purchase	CHP1	GB	CHP2	Total
Operational cost	29 575.21	12 735.80	6270.29	8741.51	57 322.81
Exergy loss	29 056.34	12 735.80	6225.41	9944.19	57 961.73

4) Comparison of Optimal Results Obtained with and without Considering Network Losses

This study conducts a comparative analysis between the proposed optimization model and a simplified model that disregards network losses. The simplified model is derived from the fundamental model introduced in this paper. However, it excludes reactive power and electricity line resistances in the electricity network and temperature drops in the heat network. In addition, power flow constraints (28)–(31) are replaced with standard DC power flow constraints [44]. However, losses associated with the charging and discharging processes of battery storage units are considered.

Figs. 14 and 15 show the optimized power and heat exergy outputs of the main equipment considering and disregarding network losses, respectively. The results obtained from the simplified model exhibit significant deviations from the proposed optimization results that account for network losses. Eliminating power network losses prevents exergy loss associated with electricity purchase and encourages higher electricity purchases during low-price (00:00–05:00) and high-demand periods (17:00–22:00), with a peak at 19:00. However, the simplified model shows a substantial reduction in electricity and heat exergy outputs from CHP2, with lower exergy efficiency. To compensate for the resulting heat energy supply gap during the 00:00–06:00 and 16:00–23:00 periods, GB and CHP1 are used. The disparities between the optimization results with and without network losses are significant, with a cumulative exergy power output deviation of 17.3357 MW and an average deviation-to-load ratio of 12.94% at each time interval.

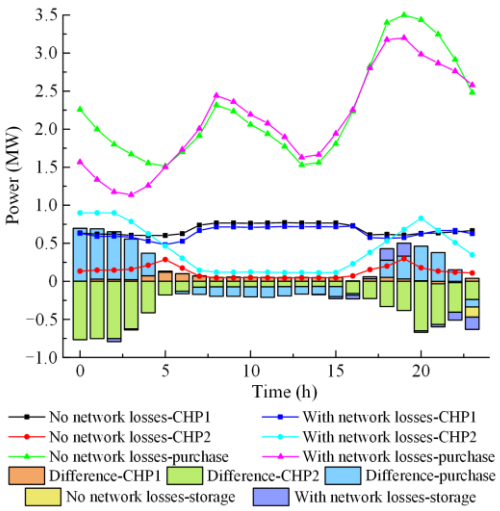

Fig. 14. Comparison of electric power exergy outputs obtained with and without considering network losses.

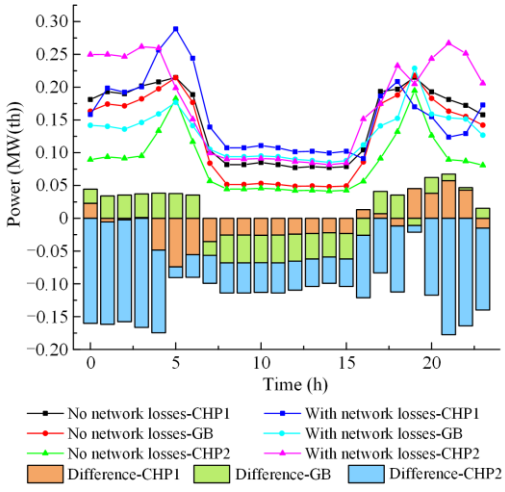

Fig. 15. Comparison of heat exergy outputs obtained with and without considering network losses.

Table V presents the exergy loss distribution at each system link with and without considering network losses. When network losses are disregarded, there is a significant reduction in exergy losses for the equipment. However, there remains a marginal level of exergy loss within the heat network because of the temperature difference in heat transfer processes at the mixing nodes, where energy flows of varying temperatures interact despite omitting heat transfer losses. In a comprehensive analysis, the exergy loss results at each link without network losses demonstrate significant deviations compared to the proposed model with network losses. The overall deviation in total exergy losses is 14.0173 MWh, constituting 27.83% of the total exergy losses.

TABLE V
COMPARISON OF THE EXERGY LOSS RESULTS OBTAINED AT EACH LINK WITH AND WITHOUT NETWORK LOSS CONSIDERATION

Loss links	With network losses (MWh)	No network losses (MWh)
GB	13.1696	9.6895
CHP2	11.7012	8.0125
CHP1	19.1068	18.3398
Supply network	2.3713	0.0814
Return network	0.8649	0.0511
Electricity network	2.9432	0
Battery storage	0.1208	0.0863
CP	0.0964	0.0964
Total	50.3743	36.3570

VI. CONCLUSION

The present work addresses the failure of current efforts to account for numerous important factors when analyzing the energy utilization efficiency of IESs. It does this by developing a unified optimal operation model-based system exergy. The model can describe the direction of exergy flows in an HE-IES and account for the effect of load rate on the energy efficiency of ECE components. Therefore the proposed model can accurately calculate the exergy loss in each link of the system. This enables the minimization of the total exergy loss of the system while also providing the exergy loss distribution of the system. The proposed optimization model is solved accurately and efficiently as an MISOCP problem by applying piecewise linearization to the non-convex terms in the objective function and the equality constraints. The main conclusions of the simulation studies are:

1) The piecewise linearization method efficiently handles the optimization model, ensuring that the maximum relative error of the solution is less than 1.2%.

2) The temperature-dependent characteristics of heat exergy provide optimization results with the minimum exergy loss objective that are essentially a trade-off between reducing the exergy loss of the system components while increasing the exergy loss of the heat network, such that the total exergy loss is minimized. From the test case conducted in this study, the reduction is approximately 3.2 times the increase.

3) The minimum exergy loss objective reverses the trend obtained under the minimum operational cost objective to reduce the total operational cost by increasing the volume of electricity purchased from the external grid during low electricity price periods and reducing the use of the GT-based CHP. Accordingly, the proposed method increases the comprehensive utilization efficiency of energy sources by increasing the use of the GT-based CHP by 13.76% rather than relying on electricity purchased from an external grid.

4) Considering network losses and minimizing total exergy loss are crucial for optimal system operation and accurate exergy loss characterization. In the simulation, the cumulative deviation in the output exergy power is 17.3357 MW, with an average deviation ratio of 12.94% relative to the load. The system's total exergy loss deviation is 14.0173 MWh, accounting for 27.83% of the total exergy loss.

Economic efficiency and energy conservation are important considerations for regional IESs. Previous studies have employed a multi-objective methodology to address these two indicators simultaneously; however, a scientific correlation for integrated optimization remains unestablished. Exergy economics offers insight into the intrinsic interrelationship between thermodynamic and economic costs associated with exergy loss. Future research will focus on optimizing the operation of HE-IESs within the framework of exergy economics. Its process may entail modeling the cost of exergy losses or pricing structures for exergy products to optimize the system's operational performance, achieving a balance between economic efficiency and energy conservation.

APPENDIX A

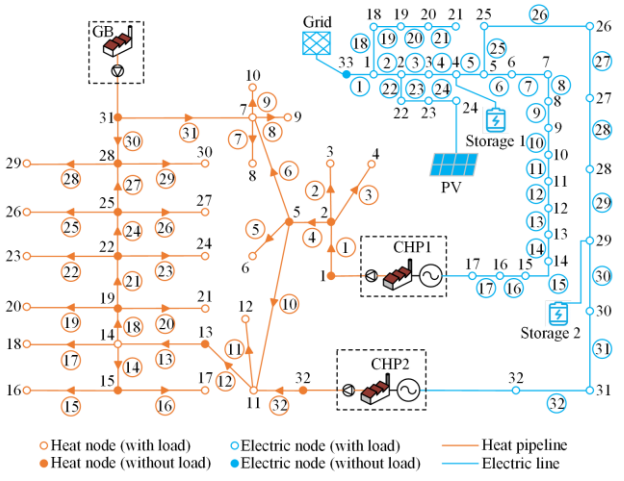

Fig. A1. Network topology of the HE-IES simulation system.

TABLE A1
EQUIPMENT PARAMETERS OF THE HE-IES

Equipment	Parameter type	Value
Gas turbine	Upper bound of electric power output (MW)	0.9
	Lower bound of electric power output (MW)	0.0045
	Maximum up-ramping, down-ramping power (MWh)	0.15, 0.16
	Coefficients	$\alpha_{GT,0}=0.089$, $\alpha_{GT,1}=0.35$ $\alpha_{GT,2}=-0.27$, $\alpha_{GT,3}=0.18$
Exhaust heat boiler	Upper bound of heat output (MW)	1.5
	Collection efficiency	0.8
Extraction steam turbine CHP	Upper bound of electric power output (MW)	0.9
	Given ratio ZST	3.8
	Maximum up-ramping, down-ramping power (MWh)	0.3, 0.3
	Electric energy efficiency	0.25
GB	Upper bound of electric power output (MW)	2
	Maximum up-ramping, down-ramping power (MWh)	0.7, 0.7
	Coefficients	$\alpha_{GT,0}=0.81$, $\alpha_{GT,1}=0.13$
Battery storage units	Maximal states of charge (MWh)	0.3, 0.2
	Upper charging, discharging bounds (MW)	0.10, 0.07
	Initial states of charge (MWh)	0.15, 0.15
	Upper bounds of apparent power (MVA)	0.1414, 0.0990
	Charging and discharging efficiency	0.93
	Energy loss coefficient	0.01

TABLE A2
PARAMETERS OF HEAT PIPELINES

Pipeline number	Length (m)	Diameter (mm)	Heat transfer coefficient (W/mK)	Friction factor	*Mass flow rate (kg/s)
1	2086.56	125	0.321	0.0271	7.1196
2	789.75	40	0.210	0.0386	1.0598
3	413.10	40	0.210	0.0385	1.3658
4	481.95	100	0.327	0.0288	4.6940
5	2197.53	32	0.189	0.0414	1.2002
6	1906.74	65	0.236	0.0328	1.2030
7	1436.13	40	0.210	0.0385	1.2276
8	832.68	40	0.210	0.0386	1.1627
9	2006.37	40	0.210	0.0385	1.2873
10	1302.48	100	0.327	0.0293	2.2908
11	1045.71	40	0.210	0.0386	1.1012
12	1507.41	100	0.327	0.0289	7.6584
13	1103.22	80	0.278	0.0307	7.6584
14	338.58	50	0.219	0.0358	1.8126
15	946.08	32	0.189	0.0415	0.8987
16	1104.84	32	0.189	0.0415	0.9140
17	1104.84	32	0.189	0.0415	0.8953
18	363.69	80	0.278	0.0309	4.1639
19	1104.84	32	0.189	0.0415	0.9063
20	1086.21	32	0.189	0.0415	0.9045
21	337.77	65	0.236	0.0329	2.3531
22	1304.91	32	0.189	0.0414	1.2280
23	1087.02	32	0.189	0.0414	1.2066
24	422.01	65	0.236	0.0349	−0.0815
25	1101.60	32	0.189	0.0414	1.0787
26	998.73	32	0.189	0.0414	1.0691
27	500.58	40	0.210	0.0384	−2.2293
28	771.12	32	0.189	0.0415	1.0230
29	851.31	32	0.189	0.0415	1.0305
30	571.86	125	0.321	0.0280	4.2828
31	2120.58	125	0.321	0.0306	3.5441
32	1630.53	125	0.321	0.0274	7.8084

*The negative sign for values in this column indicates that the flow direction is opposite to that marked on the corresponding pipeline in Fig. A1.

ACKNOWLEDGMENT

Not applicable.

AUTHORS' CONTRIBUTIONS

Jianrun Chen and Haoyong Chen: theoretical analysis and modeling of the process and performed simulation and experiment to verify the proposed method. Zipeng Liang: proposed methods for processing and solving the optimization model. Xiaodong Zheng, Dongliang Xiao, Yirui Li and Huaguang Yan: offered help in theory and practice, read and put forward suggestions for the paper. All authors read and approved the final manuscript.

FUNDING

This work is supported by the National Natural Science Foundation of China (No. 51937005).

AVAILABILITY OF DATA AND MATERIALS

Not applicable.

DECLARATIONS

Competing interests: The authors declare that they have no known competing financial interests or personal relationships that could have appeared to influence the work reported in this article.

AUTHORS' INFORMATION

Jianrun Chen received the B.S. degree in electrical engineering and its automation from the South China University of Technology, Guangzhou in 2020. He is currently pursuing the Ph.D. degree in electrical engineering with South China

University of Technology, China. His research interests include modeling, optimization, and evaluation of integrated energy system.

Haoyong Chen received the B.S., M.S., and Ph.D. degrees in electrical engineering from Xi'an Jiaotong University, Xi'an, China, in 1995, 1997, and 2000, respectively. Currently, he is a Professor with the School of Electric Power, South China University of Technology, Guangzhou, China. His major research interests include modeling of integrated energy system, power system optimal operation/planning, and power markets.

Zipeng Liang received the B.S. and M.S. degrees in electrical engineering from the South China University of Technology, Guangzhou, China, in 2016 and 2019, respectively. He is currently pursuing the Ph.D. degree in electrical engineering with Hong Kong Polytechnic University, China. His current research interests include the energy management of hybrid AC/DC microgrids, power system planning and operation with high renewable energy penetration.

Xiaodong Zheng received the B.S. degree from the South China University of Technology, Guangzhou, China, in 2015, and the Ph.D. degree from the same institute in 2020, both in electrical engineering. He is an Associate Professor with the School of Electric Power Engineering, South China University of Technology. His research interests include (distributionally) robust optimization, distributed optimization, game theory, statistical learning, quantum computing, as well as their applications in power system operations, renewable energy integration, and electricity markets.

Dongliang Xiao received the B. S. degree from Harbin University of Science and Technology, Harbin, China, in 2013, the M.S. degree from Harbin Institute of Technology, Harbin, China, in 2015, and the Ph.D. degree from University of Nebraska-Lincoln, Lincoln, USA, in 2019. He is currently a Postdoctoral Fellow with the Department of Electric Power, South China University of Technology, Guangzhou, China. His research interests include power and energy system optimization, electricity markets and risk management, and renewable energy integration in smart grid.

Yirui Li received the B.S. degree in automation from the Tianjin University, Tianjin in 2021. He is currently pursuing the M.S. degree in electrical engineering with South China University of Technology, China. His research interests include designing of electricity market, simulation and analysis of unbalanced funds.

Huaguang Yan received the M.Eng. degree in electrical engineering from Wuhan University, Wuhan, China, in 2003. He is currently the Chief Engineer with the Electricity Using and Efficiency Department, China Electric Power Research Institute. His research areas include demand side management and smart power utilization.

REFERENCES

[1] C. Klemm and P. Vennemann, "Modeling and optimization of multi-energy systems in mixed-use districts: a review of existing methods and approaches," *Renewable & Sustainable Energy Review*, vol. 135, Jan. 2021.

[2] Z. Shi, Y. Liang, and H. Li *et al.*, "Interval optimal operation of a multi-objective electric-thermal-transportation integrated energy system considering flexibility," *Power System Protection and Control*, vol. 50, no. 21, pp. 33-42, 2022. (in Chinese)

[3] J. Xu, Y. Chen, and J. Wang *et al*., "Ideal scheme selection of an integrated conventional and renewable energy system combining multi-objective optimization and matching performance analysis," *Energy Conversion and Management*, vol. 251, Jan. 2022.

[4] C. Miao, Q. Wang, and Y. Tang, "A multi-energy inertia-based power support strategy with gas network constraints," *Protection and Control of Modern Power Systems*, vol. 8, no. 1, pp. 303-320, Dec. 2023.

[5] K. Wu, J. Gu, and L. Meng *et al.*, "An explainable framework for load forecasting of a regional integrated energy system based on coupled features and multi-task learning," *Protection and Control of Modern Power Systems*, vol. 7, no. 1, pp. 349-362, Dec. 2022.

[6] J. Yang, N. Zhang, and A. Botterud *et al*., "On an equivalent representation of the dynamics in district heating networks for combined electricity-heat operation," *IEEE Transactions on Power Systems*, vol. 35, no. 1, pp. 560-570, Jan. 2020.

[7] Z. Chu, L. Zhao, and J. Sun *et al*., "Thermoelectric optimization of an integrated energy system with hydrogen energy storage considering thermal energy dynamic balance," *Power System Protection and Control*, vol. 51, no. 3, pp. 1-12, 2023. (in Chinese)

[8] D. Xu, Q. Wu, and B. Zhou *et al*., "Distributed multi-energy operation of coupled electricity, heating, and natural gas networks," *IEEE Transactions on Sustainable Energy*, vol. 11, no. 4, pp. 2457-2469, Oct. 2020.

[9] D. Wang, L. Liu, and H. Jia *et al.*, "Review of key problems related to integrated energy distribution systems," *CSEE Journal of Power and Energy Systems*, vol. 4, no. 2, pp. 130-145, Jun. 2018.

[10] P. Li, Z. Wang, and J. Wang *et al*., "Two-stage optimal operation of integrated energy system considering multiple uncertainties and integrated demand response," *Energy*, vol. 225, Jun. 2021.

[11] Y. Wang, Y. Wang, and Y. Huang *et al.*, "Planning and operation method of the regional integrated energy system considering economy and environment," *Energy*, vol. 171, pp. 731-750, Mar. 2019.

[12] J. Tan, Q. Wu, and M. Zhang *et al*., "Chance-constrained energy and multi-type reserves scheduling exploiting flexibility from combined power and heat units and heat pumps," *Energy*, vol. 233, Oct. 2021.

[13] M. J. Moran, H. N. Shapiro, and D. D. Boettner *et al.*, *Fundamentals of Engineering Thermodynamics*. John Wiley & Sons, 2010.

[14] O. Mahian, M. R. Mirzaie, and A. Kasaeian *et al*., "Exergy analysis in combined heat and power systems: a review," *Energy Conversion and Management*, vol. 226, Dec. 2020.

[15] V. İncili, G. K. Dolgun, and A. Keçebaş *et al*., "Energy and exergy analyses of a coal-fired micro-CHP system coupled engine as a domestic solution," *Energy*, vol. 274, Jul. 2023.

[16] K. Braimakis, D. Magiri-Skouloudi, and D. Grimekis *et al.*, "Energy-exergy analysis of ultra-supercritical biomass-fuelled steam power plants for industrial CHP, district heating and cooling," *Renewable Energy*, vol. 154, pp. 252-269, Jul. 2020.

[17] A. Allen, G. Henze, and K. Baker *et al*., "Evaluation of low-exergy heating and cooling systems and topology optimization for deep energy savings at the urban district level," *Energy Conversion and Management*, vol. 222, Oct. 2020.

[18] C. R. Reddy, M. Shahbakhti, and R. D. Robinett *et al*., "Exergy-wise predictive control framework for optimal performance of MicroCSP systems for HVAC applications in buildings," *Energy Conversion and Management*, vol. 210, Apr. 2020.

[19] M. Razmara, M. Maasoumy, and M. Shahbakhti *et al*., "Optimal exergy control of building HVAC system," *Applied Energy*, vol. 156, pp. 555-565, Oct. 2015.

[20] M. F. Tahir, H. Chen, and G. Han, "Exergy hub based modelling and performance evaluation of integrated energy system," *Journal of Energy Storage*, vol. 41, Sep. 2021.

[21] M. F. Tahir, H. Chen, and G. Han, "Evaluating individual heating alternatives in integrated energy system by employing energy and exergy analysis," *Energy*, vol. 249, Jun. 2022.

[22] M. F. Tahir, H. Chen, and G. Han, "A comprehensive review of 4E analysis of thermal power plants, intermittent renewable energy and integrated energy systems," *Energy Reports*, vol. 7, pp. 3517-3534, Nov. 2021.

[23] L. Mo, X. Liu, and H. Chen *et al*., (2023, Jun.), "Exergy-economic analysis and evaluation method of park-level integrated energy system," *Frontiers in Energy Research*. [Online]. Available: https://www.frontiersin.org/articles/10.3389/fenrg.2022.968102

[24] J. Li, D. Wang, and H. Jia *et al*., "Mechanism analysis and unified calculation model of exergy flow distribution in regional integrated energy system," *Applied Energy*, vol. 324, Oct. 2022.

[25] M. Sheikholeslami, M. Jafaryar, and S. Saleem *et al*., "Nanofluid heat transfer augmentation and exergy loss inside a pipe equipped with innovative turbulators," *International Journal of Heat and Mass Transfer*, vol. 126, pp. 156-163, Nov. 2018.

[26] X. Hu, H. Zhang, D. Chen *et al.*, "Multi-objective planning for integrated energy systems considering both exergy efficiency and economy," *Energy*, vol. 197, Apr. 2020.

[27] X. Hu, C. Shang, M. Wen *et al.*, "Integrated modelling and planning of regional integrated energy systems based on exergy analysis," in *8th Renewable Power Generation Conference (RPG 2019)*, Shanghai, China, Oct. 2019, pp. 295-303.

[28] M. Di Somma, B. Yan, N. Bianco *et al.*, "Multi-objective design optimization of distributed energy systems through cost and exergy assessments," *Applied Energy*, vol. 204, pp. 1299-1316, Oct. 2017.

[29] Y. Wang, F. Huang, S. Tao *et al.*, "Multi-objective planning of regional integrated energy system aiming at exergy efficiency and economy," *Applied Energy*, vol. 306, Jan. 2022.

[30] H. Li, B. Sun, and C. Zhang, "Capacity design of a distributed energy system based on integrated optimization and operation strategy of exergy loss reduction," *Energy Conversion and Management*, vol. 231, Mar. 2021.

[31] Y. Huang, Y. Wang, and N. Liu, "A two-stage energy management for heat-electricity integrated energy system considering dynamic pricing of Stackelberg game and operation strategy optimization," *Energy*, vol. 244, Apr. 2022.

[32] J. Liu, L. Ma, and Q. Wang, "Energy management method of integrated energy system based on collaborative optimization of distributed flexible resources," *Energy*, vol. 264, Feb. 2023.

[33] C. Chen, X. Shen, and Y. Xue *et al*., "A multi-objective evaluation method for distributed integrated energy system," in *2017 IEEE Conference on Energy Internet and Energy System Integration (EI2)*, Beijing, China, Nov. 2017, pp. 1-6.

[34] M. Ghorab, "Energy hubs optimization for smart energy network system to minimize economic and environmental impact at Canadian community," *Applied Thermal Engineering*, vol. 151, pp. 214-230, Mar. 2019.

[35] Y. Mu, W. Chen, and X. Xu *et al.*, "A double-layer planning method for integrated community energy systems with varying energy conversion efficiencies," *Applied Energy*, vol. 279, Dec. 2020.

[36] S. He, N. Liu, and C. Sheng *et al*., "Distributed optimal scheduling for minimizing exergy loss based on Joint operation of multiple energy hubs," *Automation of Electric Power Systems*, vol. 45, no. 9, pp. 28-37, 2021. (in Chinese)

[37] H. Chen, S. Chen, and M. Li *et al*., "Optimal operation of integrated energy system based on exergy analysis and adaptive genetic algorithm," *IEEE Access*, vol. 8, pp. 158752-158764, Sep. 2020.

[38] A. Gabash and P. Li, "Active-reactive optimal power flow in distribution networks with embedded generation and battery storage," *IEEE Transactions on Power Systems*, vol. 27, no. 4, pp. 2026-2035, Nov. 2012.

[39] X. Liu, J. Wu, and N. Jenkins *et al*., "Combined analysis of electricity and heat networks," *Applied Energy*, vol. 162, pp. 1238-1250, Jan. 2016.

[40] M. Carvalho, L. M. Serra, and M. A. Lozano, "Optimal synthesis of trigeneration systems subject to environmental constraints," *Energy*, vol. 36, no. 6, pp. 3779-3790, Jun. 2011.

[41] E. Kenna and P. Bannister, "Simple, fully featured boiler loop modelling". in *Eighth International IBPSA Conference*, Glasgow, Scotland, Jul. 2009.

[42] W. Wei, J. Wang, and N. Li *et al*., "Optimal power flow of radial networks and its variations: a sequential convex optimization approach," *IEEE Transactions on Smart Grid*, vol. 8, no. 6, pp. 2974-2987, Nov. 2017.

[43] M. Farivar and S. H. Low, "Branch flow model: relaxations and convexification—Part I," *IEEE Transactions on Power Systems*, vol. 28, no. 3, pp. 2554-2564, Aug. 2013.

[44] F. Li and R. Bo, "DCOPF-based LMP simulation: algorithm, comparison with ACOPF, and sensitivity," *IEEE Transactions on Power Systems*, vol. 22, no. 4, pp. 1475-1485, Nov. 2007.